3D Printed Blood-Brain Barrier-on-a-Chip

Agnes Dobos

under the supervision of

Prof. Aleksandr Ovsianikov

Institute of Material Science and Technology (E308)

Technische Universitat Wien

Vienna, Austria

And

Prof. Ali Khademhosseini

California Nanosystems Institute

University of California

Los Angeles, California, USA

1 TABLE OF CONTENTS

2 INTRODUCTION

Over 90% of the clinical trials fail due to inefficiency and unexpected side-effects and this has been linked partially to the currently available animal models and their capacity to mimic human conditions. Additionally due to ethical concerns, the 3R principle as in to reduce, replace and refine animal testing to provide a more humane research environment has been introduced in the last few decades [1]. One of the main bottlenecks of current drug development is the lack of available and relevant *in vitro* models. Most of the traditional *in vitro* research has been performed in 2D planar cell culture. There has been an increasing evidence that 2D cell culturing conditions do not recapitulate the complexity of the physiological 3D environment [2]. 2D cell culture experiments often present increased drug response compared the 3D cell culture which could lead to an overestimation of the efficiency of the drug [3]. There are multiple different ways to produce 3D cell culture to home cells. One of the methods often referred to as bottom up tissue engineering, employs the cells without any mechanical support using the capability of cells to self-assemble to form cell aggregates (spheroids). The production of these spheroids can be performed either by using non-adhesive (agarose or coated) plates or hanging drop cultures, etc. [4]. Top down production of 3D cell cultures involves the use of cell supporting scaffolds. These scaffolds provide mechanical strength, architecture and support to the cells. The scaffolds can be derived from decellularized extracellular matrix element or synthetic materials.

Organ-on-chip (OoC) models aim at the fabrication of physiologically relevant models of certain tissues, organs or diseases. OoCs incorporate microfluidic technology and (3D) cell culture to gain more understanding in the physiological and pathological processes. It is clear that there is an increasing need for such devices as these systems have possibility to use human cells instead of animals to recapitulate human conditions better and also the patient's own cells could be utilized, which could be a step towards more personalized medicine [5]. The microfluidics technology enables the control over many different parameters such as concentration gradients, offers continuous supply of fresh nutrients and removal of metabolites while providing mechanical stimulus for the cells. However, creating such complex designs presents a series of challenges including engineering tasks to create the cost-effective and high-throughput production of chips, scaling issues to maintain the architecture and the function of the organ model, and due to the small volume size, the optimization of analytical measurement which need to be carried out needs to be determined [6].

Glioblastoma multiforme (GBM), originated from glial cells in the brain, is the most frequent brain tumor (representing 80 % of primary malignant central nervous system (CNS) tumors) with high mortality and recurrence rate, with a median overall survival rate of 12-18 months after diagnosis [7]. The most commonly used therapy to treat GBM includes a surgical resection of the tumor with subsequent treatment with radiotherapy and chemotherapy using temozolomide (TMZ). However, this treatment scarcely increases the median survival rate as the removal of the primary tumor without damaging the brain is often not easy due to infiltrating cells in the healthy tissue [8]. Some of the other possible treatments or approaches under development include targeted therapy of the tumor, immunotherapy, antiangiogenic drugs, nanotherapy, gene therapy and electromagnetic radiation [9]. There are several challenges to face when developing more efficient treatments for GBM. There are only a very few available *in vitro* models of GBM to study the disease progression and develop new therapies [10]. Most of the preclinical studies are carried out by using rodent models, which as discussed earlier, often does not represent the human conditions efficiently. Additionally, the drug delivery strategies need to be improved as the blood-brain barrier (BBB) often poses a barrier, which prevents the intravenously or orally administered drugs to reach their target. BBB is a selectively permeable interface which separates the blood from the brain parenchyma. BBB is composed of brain endothelial cells in the cerebral microvasculature. The BBB is characterized by tight junction which leads to the formation of a capillaries which are up to 100 times tighter than peripheral microvessels. On the other side of the capillary different glial cells such as astrocytic glia cell and pericytes are present [11]. Their influence on the BBB has been demonstrated by implanting astrocytes to other sites with leaky vessels and they induced the tightening of the endothelium [12]. Between the endothelial cells and the astrocytes, a basement membrane which consists of extracellular matrix elements such as collagen, elastin, laminin, fibronectin and proteoglycans, embedded pericytes can be found [13]. This barrier has an important role to protect the brain from possibly toxic substances while maintaining the exchange of nutrients, gases, and metabolites between the blood and brain. Small molecules can diffuse through the barrier without restrictions while larger molecules need to be transported across the membrane [14]. Modeling the BBB is highly important for screening potential drug candidates for the treatment of diseases of the CNS including GBM and to study the *in vitro* drug transport across the BBB [15]. The disruption of the BBB can be found in multiple diseases including stroke, multiple sclerosis, encephalitis, brain tumors, and Alzheimer's Disease [16].

In vitro BBB models can provide valuable tools to study the physiological function and disease progression. These microfluidic based designs can implement physiologically relevant blood pressure and shear stress. Most of the chip designs used for BBB models in literature are based on polydimethylsiloxane PDMS

devices incorporated with a porous transwell membranes. Booth et al. used a co-culture of mouse endothelial cell line b.End3 together with D1A astrocytes on a 10 µm thick polycarbonate membrane with 0.4 µm pore size, and they found that the trans-endothelial electrical resistance (TEER) exceeded the monoculture of endothelial cells when co-culture was used and the and the tight junction formation was clearly visible [17]. Griep et al. used a similar PDMS device with transwell membrane with smaller pore size (8µm) coated with collagen and seeded with human brain endothelial cells (hCMEC/D3) [18]. Kim et al. presented a collagen-based microvasculature model using microneedles and 3D printed frames. The created hollow tubes were seeded with bEnd.3 cell line to create the BBB. They were able to cultivate the cells for 14 days [19]. A modular approach where the endothelial and the neuronal chambers can be cultivated separately and assemble at a later time point was demonstrated by Achyuta et al. [20]. Ma et al. and co-workers fabricated BBB chips employing low-stress silicon nitrid membranes with 400 µm pores produced by either a lithographic stepper or an electron beam lithography system and was further modified by spinning collagen type I onto the membrane to improve cell attachment. This membrane was later seeded with primary rat astrocytes on one side and immortalized brain capillary endothelial cell line SV-HCEC on the other side to study the contribution of the different cells on the resistance on the fabricated membrane [21]. Brown et al. has designed a NeuroVascular Unit (NVU) to recpitulate the function of the BBB. The NVU produced by three PDMS layers separated with polycarbonate membrane with 0.2 µm pore size. The membranes were coated with laminin prior cell culture use. Primary human brain-derived microvascular endothelial cells (hBMVEC), primary astrocytes and pericytes and human induced pluripotent stem cells (hiPSCs) differentiated into human cortical glutamatergic neurons were used throughout the experiments. They were able to maintain cell viability on the chip for over 3 weeks of culture. They compared the effect of different cell culture media and flow to improve to tight junction formation of the endothelial cell layer and examined the tranport of different sized molecules across the membrane [22]. Deosarkar et al. has employed a PDMS device and replaced the standard polycarbonate membranes by producing a series of 3 µm pores along the vascular channels to create a dynamic neonatal BBB on a chip. Neonatal rat brain capillary endothelial cells (RBEC) and primary cultures of neonatal rat astrocytes were seeded on the fibronectin coated device and were cultured for 5 days. Their results showed that the permeability of their chip was significantly lower compared to conventional transwell BBB models [23]. Wang et al. differentiated hiPSCs into microvascular endothelial cells and co-cultured them together with rat primary astrocytes. They have evaluated the transport of several different sized molecules and drugs such as caffeine, cimetidine, and doxorubicin [24].

Although there are multiple relevant BBB models are available in literature to study drug transport through the BBB, only a very few GBM-on-chip devices were reported which could be used to evaluate the efficiency of the possible treatments. M. Akay and co-workers have produced brain cancer chips using two U-87 and primary, tumor-derived human GBM cells to create high throughput drug-screening platforms [25], [26]. Ayoso et al. used U-251 GBM cells encapsulated into a collagen hydrogel inside a SU-8 device produced via photolithography, however, these first approached did not provide an endothelial layer to mimic the complexity of the BBB [27]. A recently published GBM-on-chip from Yi et al. employed bioprinting to create a more biomimetic *in vitro* model. Patient-derived GBM cells were used to form spheroids and were embedded in brain decellularized ECM (BdECM). After the GBM cells were printed, a vascular bioink containing human umbilical vein endothelial cells (HUVECs) embedded in BdECM were printed around the GBM to establish a vessel barrier. They have found that the patient specific cells produced different responses to the different drugs and drug combinations [28].

There are several different ways microfluidic chips can be produced [29]. One of the most commonly used methods include injection molding, laser ablation and hot embossing. During injection molding the material is formed inside a mold containing the negative and once it solidified it can be removed [30]. Many different materials can be processed using this technique including thermoplastics and thermosets as long as the viscosity of them a relatively low allowing the injection. Laser ablation is based on a breaking chemical bonds within a polymer material employing laser therefor removing material and creating channels based on a computer assisted design (CAD) [31]. During hot embossing first a master is produced then by using presses or other devices, a polymeric sheet is pressed together by a heating plate. Once the instrument cooled down, the sample can be easily removed from the mold [32]. Bioprinting and additive manufacturing technologies (AMTs) are novel methods that could enhance the development of complex OoCs in a controllable manner. Traditional extrusion based bioprinting relies on the layer by layer deposition of materials into a substrate, thereby creating a 3D structure. Cells, together with a biocompatible bioink formulation can be deposited via extrusion, inkjet or laser-assisted strategies. Although, this straightforward approach provides high control over spatial distribution of cells, one of the main limiting factors of this method that high temperature and shear stress could impair cell viability and the resolution of these printers are restricted [33]. During stereolithography a 3D construct is cured layer by layer by moving a motorized stage subsequently polymerizing a photosensitive resin via (UV) light irradiation in a bath [34]. Two-photon polymerization (2PP) is an emerging state-of the-art, high resolution bioprinting technique, where nonlinear absorption of a tightly focused, femtosecond near infrared laser pulses leads to localized cross-linking of photosensitive materials within the focal volume. Structures can

be directly produced within the bulk of the material, eliminating the need of a layer-by-layer deposition, which is required in other additive manufacturing technologies. 3D constructs with feature sizes from less than 100 nm can be fabricated [35].

Several different materials can be employed as bioinks for 2PP and other AMTs including natural and synthetic polymers. In general, synthetic polymers have a wide medical applications range, such as implants and intraocular lenses among many others [36], [37]. Some of the main advantages of such materials that they high reproducibility between batches and the chemical composition of them can be easily modified to introduce new functionalities and material properties. However the disadvantages of synthetic materials include the lack of cell-responsive moieties and biodegradation, and they are often cytotoxic [38]. Natural polymers often perform better in terms of biocompatibility and biodegradability, but they often lack control over mechanical properties and they could trigger immune responses in some cases [39]. The non-cellular component of all tissues is the ECM, which provides not only the necessary biological cues needed for cell signaling, tissue development, differentiation, proliferation, and migration but also the desired mechanical support including elasticity, tensile and compressive strength. The most commonly used natural polymers include collagen, gelatin and hyaluronic acid.

Hydrogels are polymer networks which are capable of the uptake of large quantities of water. The crosslinking of hydrogels can occur through a variety of mechanisms to form either a physical or chemical crosslinked hydrogel. During physical (reversible) crosslinking the polymer is formed by secondary forces such as hydrogen-, or ionic bonds, hydrophilic or hydrophobic forces, π-π stacking, or entanglements. One of the main advantages of these hydrogels are that they can be formed without any crosslinking additives which are often cytotoxic. On the other hand chemically crosslinked hydrogels are stabilized by covalent bonds. The chemical crosslinking of the polymer could be driven by free radicals, enzymes, Diels-Alder click reaction, Michael type addition and Schiff base formation among others.

Photopolymerization is driven by different reactive species (radicals, cations or anions). Once the reactive species is initiated by a photoinitiator (PI). PIs are substances which generate reactive species upon irradiation. Based on their mechanism of action can be either type I or type II. The type I initiators cleave to produce two radicals upon irradiation, while type II initiators undergo a bimolecular process in which the first step is abstract an electron or hydrogen atom from a second molecule (co-initiator) and in turn this molecule then reacts to initiate polymerization. There are several biocompatible PIs such as Irgacure 2959 and Li-TPO. These PIs have a good absorption in the UV region (250-370 nm), however they often have poor performance in two-photon setting. There are a few water soluble two-photon PIs (2PIs)

reported in literature, however only a very few of them presented as biocompatible for biological applications [40], [41]. Once the polymerization process is initiated by PI, the polymer network formation can occur either via chain-growth or step growth mechanism. In chain growth polymerization, the process is introduced by an initiation step followed by a propagation period where the monomer only reacts to the at the end of the growing polymer chain, and the monomer concentration is decreasing throughout the reaction, and finally a chain termination occurs. One of the most well-known chain growth polymers used in tissue engineering approaches is gelatin-methacrylate (GelMA). Traditional photopolymerization of hydrogels with (meth)acrylate functionalities have been largely employed in medical and biological applications. GelMA hydrogels are an inexpensive, biocompatible platforms for 3D cell culture applications, where the mechanical properties of the material can be fine-tuned by changing the polymer concentration. However, they often exhibit a series of restrictions including heterogeneous network formation and extensive swelling. In step-growth polymerization the monomers first form dimers, then trimers, longer oligomers and ultimately long chain polymers. Thiol-ene step growth polymers form via (photo)click reactions can overcome the limitations of the chain-growth GelMA hydrogels. Thiol-ene click reaction is based on the orthogonal reaction of thiols with carbon-carbon double bonds. The network formation proceeds by repeated addition of thiyl radials to double bonds and chain transfer reactions by hydrogen abstraction [42].

3 AIM

The goal of the project is to establish a physiologically relevant blood-brain-barrier model. A microfluidic chip using a medical grade mold material and the printing of a biodegradable and biocompatible membrane via two-photon polymerization will be established. Different cells, both on the “blood” and the “brain” compartments of the chip can be drop-seeded and perfused with their corresponding media separately. The formation of an endothelial monolayer and the cell viability of the cells in the “blood” compartment will be addressed using live/dead staining, and immunohistochemical staining using vascular endothelial cadherin (VE-Cadherin) for the visualization of adherens junctions. Additionally, the diffusion of different sized water-soluble molecules (2000 kDa, 150 kDa, 70 kDa, 4 kDa, fluorescein and riboflavin) will be tested on the 3D printed membrane. The effect of endothelial cells on the diffusion rate will be tested.

4 MATERIAL AND METHODS

All materials and chemicals are from Sigma Aldrich (St. Louis, Missouri, USA) unless stated otherwise. Graphs were plotted using GraphPad Prism 6.

4.1 GLASS FUNCTIONALIZATION

In order to ensure the adhesion of both the microfluidic mold materials and the 3D printed hydrogel membrane structures to the top and bottom of the chip, the glass surfaces were functionalized with methacrylate groups prior to the assembly of the chip. Two different glass slides, a 1.1 mm thick microscope cover slide (Carl Roth, Karlsruhe, Germany) and a high precision 170 µm thick glass slide (Ibidi GmbH, Martinsried, Germany) were used throughout the experiments. First, the glass surfaces were cleaned with 70 v/v% isopropanol and then with acetone and it was followed by 10 min of plasma treatment (Harrick plasma, Ithaca, USA). The methacrylation solution was prepared by mixing 50 v/v % deionized water, 48 v/v % ethanol and 0.3 v/v % acetic acid using a magnetic stirrer and adding 2 v/v % of 3-(trimethoxysilylpropyl)-methacrylate dropwise to the mixture. The solution was stirred for 20 min before submerging the plasma treated glass slides for 45 min. Afterwards the glass slides were washed with deionized water and dried at 65 °C. The glasses were sterilized by rinsing with 70 % isopropanol before the assembly of the chip and cell culture use.

4.2 MICROFLUIDIC CHIP PRODUCTION

The microfluidic chip was produced by adhering two glass slides, one with a thickness of 1 mm and one high precision 170 µm thick together with a double sided the tape. The glass slides were functionalized with methacrylate groups according to the previously mentioned protocol. The chip mold material used to produce the microfluidic chambers was ArCare 90445 (Adhesive Research, Glen Rock, Pennsylvania, USA). This material is based on medical grade double-sided pressure sensitive adhesive tape. The height of the mold was approximately 81 µm. The adhesive tape was cut according to the computer assisted design (CAD) to create the X shaped microfluidic chips using an XY plotter (Camm-1 GS-24, Roland DG Care, Hamamacu, Japan). The connections for the ports were created by drilling the holes into the thick glass cover slide prior to the chip assembly using a micro drill (TBM220 Typ 28128, Proxxon GmbH, Radingdorf, Germany). The protecting foil was removed from the adhesive tape and the two glass slides were bonded together. As connectors, 20-gauge bund needles were glues onto the glass using a two

component epoxy glue (Klebfix, Dip-tools, Stuttgart, Germany). For additional strength and isolation two component dental glue (Twinsil, Picodent, Wipperfürth, Germany) was applied.

4.3 Material Synthesis

Norbornene functionalized gelatin (Gel-NB) with a degree of substitution (DS) of 90% was synthesized according to a previously reported protocol.[43] Briefly, in order to produce 10 g of GelNB, first 1.6 g of 5-norbornene-2-carboxylic acid was dissolved in dry DMSO (Chem-Lab, Zedelgem, Belgium) under inert atmosphere argon (Ar). After it fully dissolved, 1.476 g (7.7 mmol) of 1.33 g (11.55 mmol) N-hydroxysuccinimide and 1-ethyl-3-(3-dimethylaminopropyl) carbodiimide (TCI Chemicals, Tokyo, Japan) was added to the reaction mixture subsequently degassing the mixture three times. Afterwards, the reaction proceeded at room temperature for 25 h to eliminate any unreacted EDC functionalities. Following, 10 g of gelatin type B was dissolved in 150 mL dry DMSO at 50°C under inert atmosphere and reflux conditions. After it fully dissolved, the previously prepared 5-norbornene-2-succimidylester mixture was added to the dissolved gelatin and the mixture was subsequently degassed three times. The reaction proceeded for 20 h followed by precipitating in acetone and the precipitate was filtrated (VWR, pore size 12 – 15 µm, Radnor, USA) on a Büchner filter. After washing the precipitate, it was dissolved in double distilled water (ρ = 18.2 MΩ cm) and dialyzed (Spectra/por 4: MWCO 12 – 14 kDa) for 24 h at 40 °C against distilled water. After dialysis, the pH of the solution was adjusted to physiological pH (7.4) using a 5 M NaOH solution. Finally, from the obtained clear solution, Gel-NB was isolated using freezing and lyophilization (Christ freeze-dryer Alpha 2-4 LSC, Martin Christ GmbH, Osterode am Harz, Germany) and was stored in room temperature.

4.4 Laser Setup

A tunable femtosecond NIR laser (MaiTai eHP DeepSee, Spectra-Physics) was used at 720 nm, with a repetition rate of 80 MHz and a pulse duration of 70 fs after the microscope objective (10x/0.3, Zeiss, Oberkochen, Germany). The hatch spacing was set to 0.5 µm and the layer spacing was 1 µm. An acousto-optic modulator (AA Opto Electronic, Orsay, France) is responsible for the fast switching of the laser, and a telecentric tube lens assembly guarantees that the focus stays at the back aperture of the objective. The sample was positioned by a motorized microscope stage. The laser positioning was attained by a galvometric scanner (intelliSCAN10, Scanlabs, Puchheim, Germany). The minimal feature size (resolution of the printing) can be contributed to the volumetric pixel (voxel). Full width half maximum (FWHM) of

the voxel for the used objectives and wavelengths were calculated by the following equations and the results can be found in (**Table 1**);[44]

$$FWHM_{x,y} = \frac{0.32\lambda}{\sqrt{2}NA} 2\sqrt{\ln 2}$$

$$FWHM_z = \frac{0.532\lambda}{\sqrt{2}} \left[\frac{1}{n-\sqrt{n^2-NA^2}}\right] 2\sqrt{\ln 2}$$

Where, λ is the applied wavelength, *NA* the numerical aperture of the objective and *n* the refractive index of the material.

Table 1. Full width half maximum (FWHM) and the resulting volume of the voxel for the objective used in this study.

Objective	Wavelength [nm]	$FWHM_{x,y}$ [µm]	$FWHM_z$ [µm]	Volume [µm^3]
10x, 0.3 NA	720	0.9	13.2	18.9

4.5 3D Printing of the Barrier-on-Chip

For the barrier printing, Gel-NB with a degree of substitution of 90% was dissolved in phosphate buffered saline solution (PBS) in a 37 °C water bath to obtain a final concentration of 7.5 wt %. After it completely dissolved, the hydrogel was supplemented with 0.5 mM of the cleavable diazosulfonate photoinitiator DAS and the di-thiol crosslinker dithiothreitol (DTT) at an equimolar thiol-ene ratio were added at last. Next, the obtained solution was pipetted into the assembled microfluidic chips, and the was left to form a physical gel at room temperature for 15 min. Once the gel was formed, different thickness membrane models were printed according to the CAD to create a barrier between the two chambers of the X chip using a laser power of 70 mW and a writing speed of 1 m s^{-1}. The samples were developed by placing the microfluidic chips into a 37 °C incubator. After 30 min incubation, the unpolymerized material was removed by a vacuum pump, and PBS were added to the two different chambers of the chip. The integrity of the printed structures was tested by adding 2000 kDa FITC-dextran (TdB Consultancy, Uppsala, Sweden) for 1 h to one side of the chip, which does not diffuse into the material.

4.6 Cell Culture

Human umbilical vein endothelial cells (HUVECs) and red fluorescently labelled HUVECs (PeloBiotech GmbH, Plantegg, Germany) were used at the "blood" compartment of the chip to create an endothelial cell layer on the membrane. The cells were cultivated in endothelial cell medium (Lonza Group AP, Basel, Switzerland) (Promocell, USA) supplemented with 5 % foetal bovine serum (FBS) and were used up to 10 passages. 50B11 nociceptive dorsal root ganglion sensory neuronal line (provided by University of California) were used on the "brain" compartment of the chip for the preliminary experiments. The cells were maintained in neurobasal cell culture media with 10 % FBS (XX). All cells were cultivated at 37 °C and 5 % CO_2 in the incubator. Upon 90 % confluency, the cells were detached using 0.5 % trypsin-EDTA solution and centrifuged at 170 g for 5 min before plating them onto T75 flasks.

4.7 Cell Seeding and Perfusion Setup

After the membrane barrier was printed and developed, it was equilibrated in cell culture media for 24 h prior to the seeding of cell. First, the cells for the brain compartment of the chip (50B11 cells) were detached by 0.5 % Trypsin-EDTA and the cells were centrifuged for 5 min at 170 g before resuspending it in the concentration of 1 million per mL. The cells were seeded onto the membrane and were left to adhere for 2h. For the "blood" compartment endothelial cells were drop-seeded onto the membrane and were left to adhere for 24h. The diffusion of different molecules was tested 2 days after seeding.

4.8 FITC-Dextran Diffusion

The integrity of the printed membrane was tested with 2000 kDa dextran-FITC dissolved in PBS at a concentration 0.5 mg mL^{-1}. The diffusion of different molecular sized FITC-dextran (4 kDa, 70 kDa and 150 kDa) (TdB Consultancy, Uppsala, Sweden) riboflavin (0.38 kDa), fluorescein (0.4 kDa), FITC-albumin molecules using the same concentration were recorded using LSM 800 for 1 h at 37 °C both as membrane alone and membrane with cells. ImageJ software was used analyze the fluorescence intensity in the different compartments of the chip.

4.9 Live-Dead Staining and Immunostaining

In order to assess the cell viability after drop-seeding the cells were stained with Calcein AM/Propidium iodide (PI) live-dead staining according to the manufacturers protocol for 30 min. In short 1: 2500 of PI

and 1: 10 000 of Calcein AM dilution of the staining solution was prepared in cell culture media and were added to the microfluidic chip. The cells were imaged using LSM 800. After imaging, the cell culture media was changed and the cell staining was repeated if needed at a later time point. The number of dead and alive cells were counted manually.

24 h after seeding the cells in the control static and the perfused samples, the samples were fixed with 4 % Histofix (Carl Roth GmbH, Karlsruhe, Germany) for 1 h. Next, the cells were washed with PBS twice. The permeabilization was accomplished by incubating the samples with 0.5 % Triton-X in 1 wt % bovine serum albumin dissolved in PBS (PBS-BSA) for 5 min. Next, anti-VE Cadherin antibody (Thermo-Fisher, Waltham, MA, USA) in a dilution of 1:500 was added for 2 h at room temperature. Afterwards, the constructs were washed for 15 min with PBS-BSA before the addition of the Goat anti-Rabbit IgG Superclonal Secondary Antibody, Alexa Fluor 488 (Thermo-Fisher, Waltham, MA, USA) in a dilution of 1:1000 for 2h. Next, the structures were washed again for 15 min with PBS-BSA before the addition of DAPI in a dilution of 1:200 in PBS-BSA for 1 h.

5 Results and Discussion

5.1 Chip Production

Most of the currently available BBB models almost exclusively rely on the use of PDMS devices. PDMS is a widely used polymer used in soft lithography to produce a model of the mould which can later be bound to glass surfaces after plasma treatment. The main advantages of PDMS include that it is transparent at the 240 nM – 1100 nM range and has a low autofluorescence allowing the optical imaging of the device, it is biocompatible and gas permeable, and has a relatively low cost [45], [46]. However, it is known that PDMS can absorb certain small molecules and incompletely crosslinked PDMS could leach into the created channels which could alter the results of the experiments [47], [48]. Our aim was to employ a pressure sensitive adhesive double-sided tape to cut out the desired geometry and adhere it in between glass slides (**Figure 1A**). This medical grade film has a height of 81 µm and contains an inert, non-migratory acrylic adhesive to ensure the attachment to the glass. An X geometry was cut out of the adhesive film in order to have separated compartment after printing of the membrane. In the middle part of the X chip, the distance between the walls of the mould was set to 1500 µm, which was chosen to ensure that the

membrane can be produced directly on the chip by printing a single membrane, as distances larger than 1500 µm would be larger than the field of view of the used objective therefore it would require a stitching step. However, this step could increase both the time needed for the membrane printing and also the failure rate as well. The high precision 170 µm thick glass bottom of the chip allows both the high-definition 3D printing of the barrier directly on the chip and also the optical imaging of the chip afterwards. The holes for the ports were drilled into the top glass microscope slide. Once the chip is assembled, the reservoirs and connectors can be glued onto the top glass using a dual component, water resistant epoxy glue which cures at room temperature in 1 h (**Figure 1B**). Two different components were used, for the blood compartment a bunt needle was glued to allow the perfusion of the system, while for the brain compartment, which needs to be cultured under static environment, a closable reservoir was attached to maintain sterile cell culturing condition and enable easy media exchange. By using the pressure sensitive double-sided adhesive tape as a mould material, the production time of a single chip can be achieved in minutes.

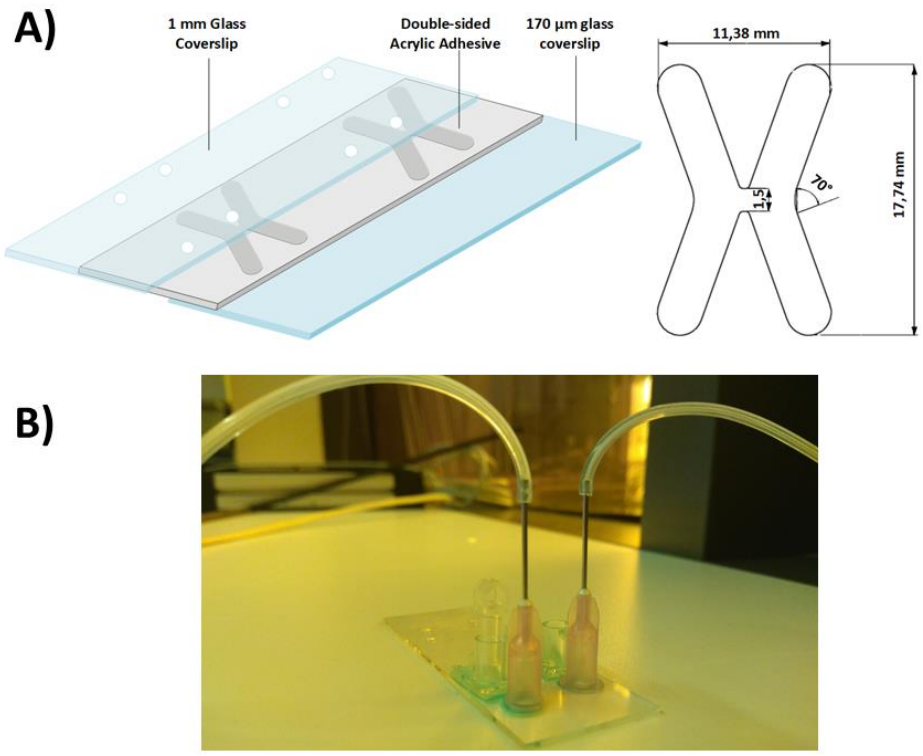

Figure 1. Microfluidic chamber design. A) Schematic design of the microfluidic chamber with the measurements of the adhesive mould B) the assembled chip with the reservoirs and connectors.

5.2 Membrane Printing and the Effect of Thickness on the Permeability

The production of PDMS based BBB usually require a multi-step chip assembly process in which usually polycarbonate membranes with large pore sizes are introduced between the layers. One of engineering challenges in such a process is the reproducible and high throughput production of the microfluidic devices, and to ensure that the membrane is tight and not leaking which is especially crucial for creating barrier models. Two-photon polymerization based high definition (HD) bioprinting of membranes directly on the chip could reduce the time and effort needed to produce these microfluidic devices. Once the mould is assembled the channels can be filled up with the photosensitive monomer solution together with a 2PI and the barrier can be printed according to a CAD. The unpolymerized material can be removed by a simple washing step. This technology also allows the processing of naturally derived hydrogels to avoid the use of plastic membranes in the device. HD bioprinting of hydrogels using gelatin based thiol-ene photo click hydrogel (Gel-NB) has been demonstrated previously using a diazosulfonate based 2PI [49]. These hydrogels have excellent biocompatibility both as a bioink as a scaffold material. Furthermore, it is fully biodegradable, and it is possible to achieve different stiffnesses depending on the applied laser power.

For the BBB model a looped structure was designed to increase the surface area of the barrier. The high-throughput production of the membrane was ensured by a high writing speed of 1 m s^{-1} resulting in that a single membrane can be produced under 5 min. The tightness of the membrane was tested by adding 2000 kDa FITC-Dextran to one of the compartments and image the fluorescence signal in the two separated channels as this molecule is unable to penetrate the hydrogel (**Figure 2**). The effect of the thickness of the membrane on the permeability of different sized molecules were tested. Two different thickness membranes, one with 30 µm (**Figure 3A**) and 60 µm (**Figure 3B**) were printed. First the transport of a small molecule, riboflavin (Mw: 376 g mol^{-1}) was tested. The results show that although riboflavin passed through the 30 µm membrane faster, the difference was not significant compared to the 60 µm membrane (**Figure 3C**). On the other hand, when 70 kDa FITC-Dextran was used, the diffusion was further impaired at later timepoints while there was no significant difference after the first hour (**Figure 3D**).

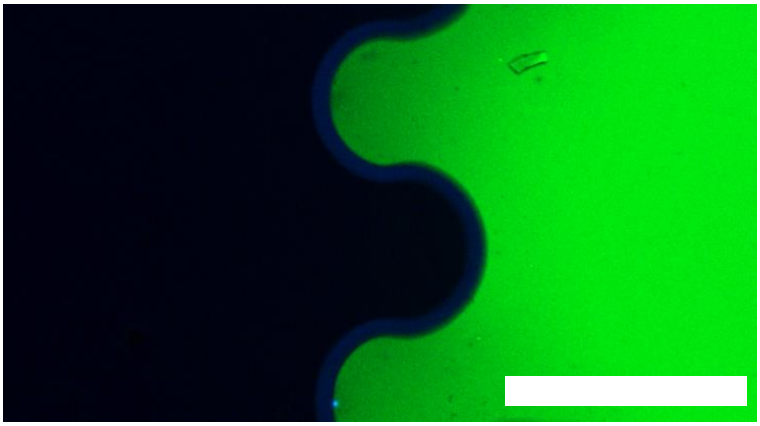

Figure 2. 30 µm thick membrane one week after printing after. The right side is filled with 2000 kDa FITC-Dextran. The fluorescent substance did not diffuse to the adjacent compartment of the chip. The scale bar represents 500 µm.

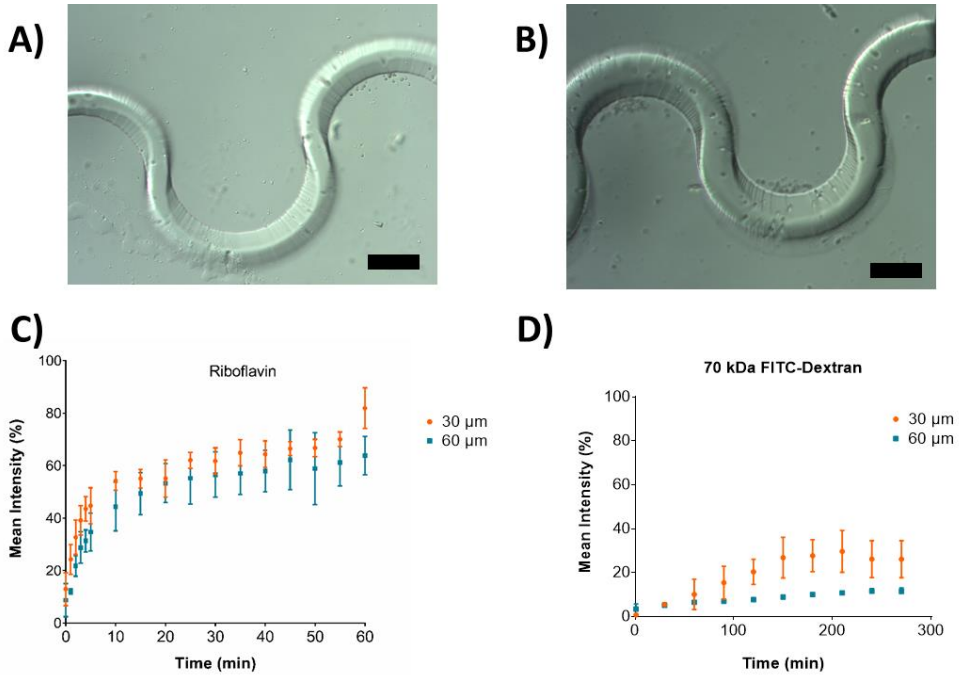

Figure 3. Printing of different thickness membranes and their effect on the permeability. Bright field microscopy image of a A) 30 µm B) 60 µm thick looped membrane. C) The diffusion of riboflavin and D) diffusion of 70 kDa FITC-dextran through the barrier. The thickness did not significantly alter the diffusion rates under 1 h for either substances. The diffusion of the larger molecules over extended period of time showed dependency on the membrane thickness. All experiments were performed in triplicates. The scale bar represents 100 µm.

5.3 Characterization of Membrane Permeability

The permeability of the membrane was characterized by tracking the diffusion of different sized molecules across the barrier. For this use, fluorescent substances with molecular weights ranging from 0.38 to 150 kDa were applied and the fluorescence intensity in the two different compartments were imaged every 5

min for 1 h. Our results showed that approximately 2 % of the large molecular weight dextran (150 kDa and 70 kDa FITC-Dextran) were able to cross the barrier after 1 h. However, almost nearly 8 % of the FITC-Albumin were able to penetrate the membrane, although the molecular weight of FITC-Albumin (66 kDa) is comparable to the 70 kDa dextran. This could be explained by the hydrodynamic radius of the substances, which can be measured via several different methods, such as light scattering. Polysaccharides such as dextran have larger hydrodynamic radii than the globular proteins for instance albumin. Previous research showed that the hydrodynamic radius of FITC-albumin is 5.4 nm ± 0.1, while 70 kDa FITC-dextran is around 6 nm, therefore it could pass through the barrier faster [50], [51]. The bain to blood ratio of 4 kDa FITC-dextran was nearly 0.4, while the small substances such as fluorescein and riboflavin reached 0.9 and 0.8, respectively (**Figure 4**). The 2000 kDa FITC-dextran with a hydrodynamic radius of 19.50 ± 1.29 nm were unable to enter the hydrogel, suggesting that the pore size of the hydrogel was smaller than 20 nm [52].

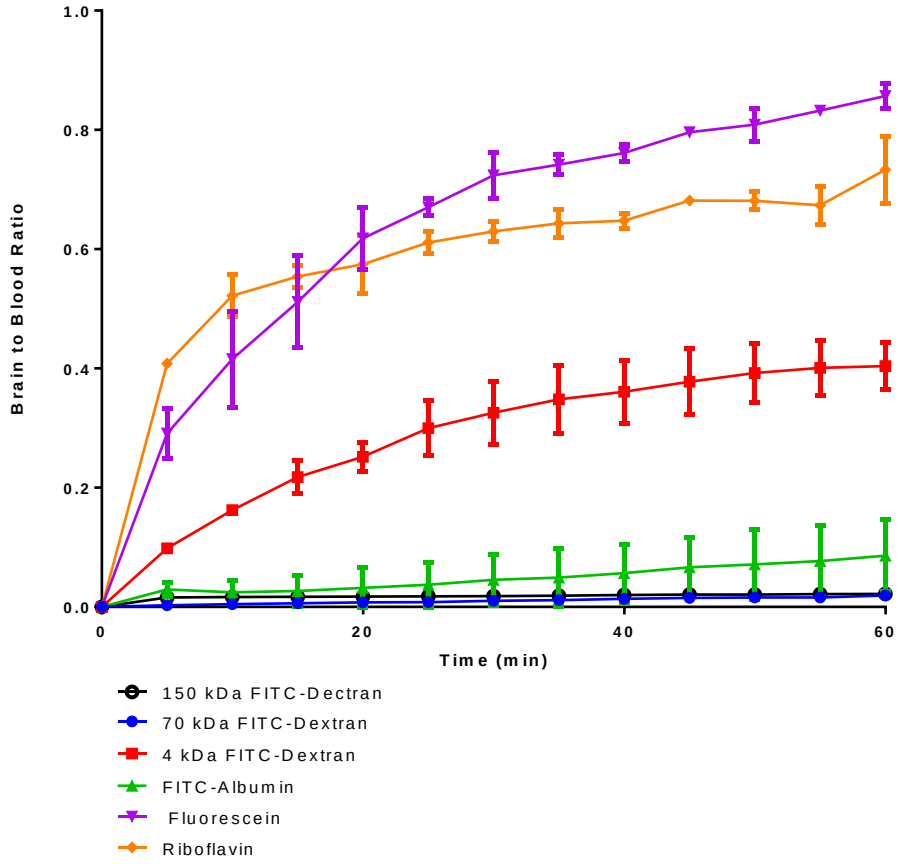

Figure 4. Permeability of the membrane to different sized molecules. Small molecules such as riboflavin and fluorescein diffused through the membrane quickly. Larger molecules (4 kDa, FITC-albumin, 70 and 150 kDa FITC-dextran) diffused through the membrane in a reduced rate. All experiments were performed in triplicates.

5.4 Cell Viability

The BBB comprises of two main cell types, vascular endothelial cells on the blood side of the barrier and glial cells adjacent to it. For the preliminary studies, human umbilical vein endothelial cells (HUVECs) were used on the blood compartment and on the brain compartment nociceptive dorsal root ganglion sensory neuronal line (50B11) was seeded. First, the 50B11 cells were drop seeded onto the membrane and were left to sediment and adhere to the membrane for 2 h while incubating the chip vertically. Once the cells adhered, the cells not attached were removed and the process was repeated with HUVECs on the other side. After two days the cells were stained using Calcein-AM and propidium iodide (PI) live-dead staining and the cells were imaged with confocal laser scanning microscope. The live cells stain green, while the dead cells can be visualized in red. The results show that after two days the cells were forming a monolayer on both sides of the membrane and they maintained their cell viability (**Figure 5**). There were no visible

dead cells on the chip, possibly due to their removal during changing the media. These results indicate that the bioprinted Gel-NB hydrogel barrier supports cell adhesion and proliferation without the need of any additional coating and can be used directly after fabrication.

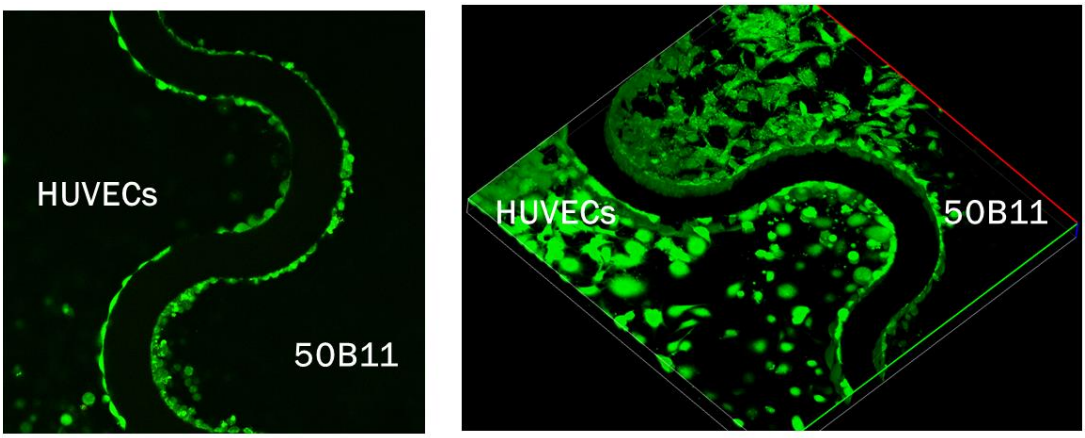

Figure 5. Live-Dead staining of cells cultured on the printed membrane. The green cells represent live cells. On the blood compartment human umbilical vein endothelial cells (HUVECs) and on the brain compartment nociceptive dorsal root ganglion sensory neuronal line (50B11) were seeded. The staining was performed 2 days after seeding.

5.5 Characterization of Membrane Permeability in the Presence of Cells

The effect of the presence of endothelial cells on the diffusion of different sized molecules were evaluated using the previously mentioned fluorescent substances. HUVECs were seeded onto the membrane and were cultivated for 2 days prior to the experiments. Afterwards, the fluorescent substances were pipetted into the blood compartment of the device and the fluorescent signal was recorded every 5 min at 37 °C for 1 h. HUVECs significantly decreased the permeability of the membrane to all the tested substances (**Figure 6**).

A previous *in vitro* study introduced 10 (w/v)% sodium fluorescein to the animal models and was left to circulate for 10 min. Afterwards, the brain tissue was homogenized and the fluorescence levels were normalized against the serum concentration [53]. Their results showed an uptake of fluorescein of approximately 0.05 which is three folds lower than the concentration measured in our system with HUVECs (blood to brain ratio of 0.15). We hypothesize that this could be due to insufficient and immature intercellular junction formation after 2 days. Additionally, the fluorescence in the *in vivo* model was analyzed in the brain tissue homogenate, while we only look at the accumulation of the fluorescent dye next to the membrane. After 1 h the brain to blood ratio of fluorescein in the case of membrane alone

reached nearly 0.9, while in the presence of cells it was 0.65 at the same time point. In another *in vivo* study, 4 kDa FITC-dextran was injected into the tail vein of mice and was left to circulate for 5 min. Afterwards, the animals were sacrificed and blood was collected as a control. The brain was extracted and the fluorescence of FITC-dextran in the cerebrum was compared to the control. Their results showed a ratio was between 0.001 and 0.0013 [54]. Our results with endothelial cells had ten-fold higher diffusion with a mean ratio of 0.013 after 5 min, while the barrier alone had a ratio of 0.1. Albumin a highly water-soluble globular protein which can be commonly found in the blood plasma. Previous studies have shown that albumin does not enter the brain parenchyma and stays inside the brain microvessels [55], [56]. Our results have shown that the presence of the cells the diffusion of FITC-albumin was 10-fold decreased compared to the membrane alone reaching 0.01 brain to blood ratio after 1 h. However, the signal reached its maximum after 30 min and did not increase significantly at later time points. Earlier studies show that the healthy BBB is largely impermeable to 70 kDa FITC-dextran in vivo. Our results after 1 h presented a fluorescence brain to blood ratio of less than 0.006 in the presence of cells, over three-folds less than the barrier alone. Studies using BBB-on-a-chip models exhibited similar finding to our results using a monoculture of endothelial cells and incubating them with 4 kDa and 70 kDa FITC-dextran. However, the increased barrier function was described when co-culture of the cells were used [17].

After the contribution of the endothelial cells alone were established, 50B11 cells were seeded onto the brain compartment of the chip. The cells were incubated and the diffusion riboflavin was tested at different time points. Riboflavin is a water-soluble vitamin (also known as B2). The uptake mechanism of riboflavin into the brain has been unclear. A previous study which employed immortalized rat brain endothelial cells (RBE4) to study the uptake of riboflavin hypothesized that riboflavin uptake is transported via carrier mediated transport system and is dependent on several different factors including sodium levels and temperature [57]. There was also evidence that the process is saturable in the micromolar range which is in good correspondence with our result where a plateau stage is reached after 20 min in the day 3 sample. Our results have further shown that after one day the diffusion of riboflavin is higher than after 3 days, possibly due to low cell numbers and immature intercellular junction formation. After 5 days the permeability of the system increases again and additionally the standard deviation between samples are increased, possibly due to decreased cell viability under static condition over an extended period of time.

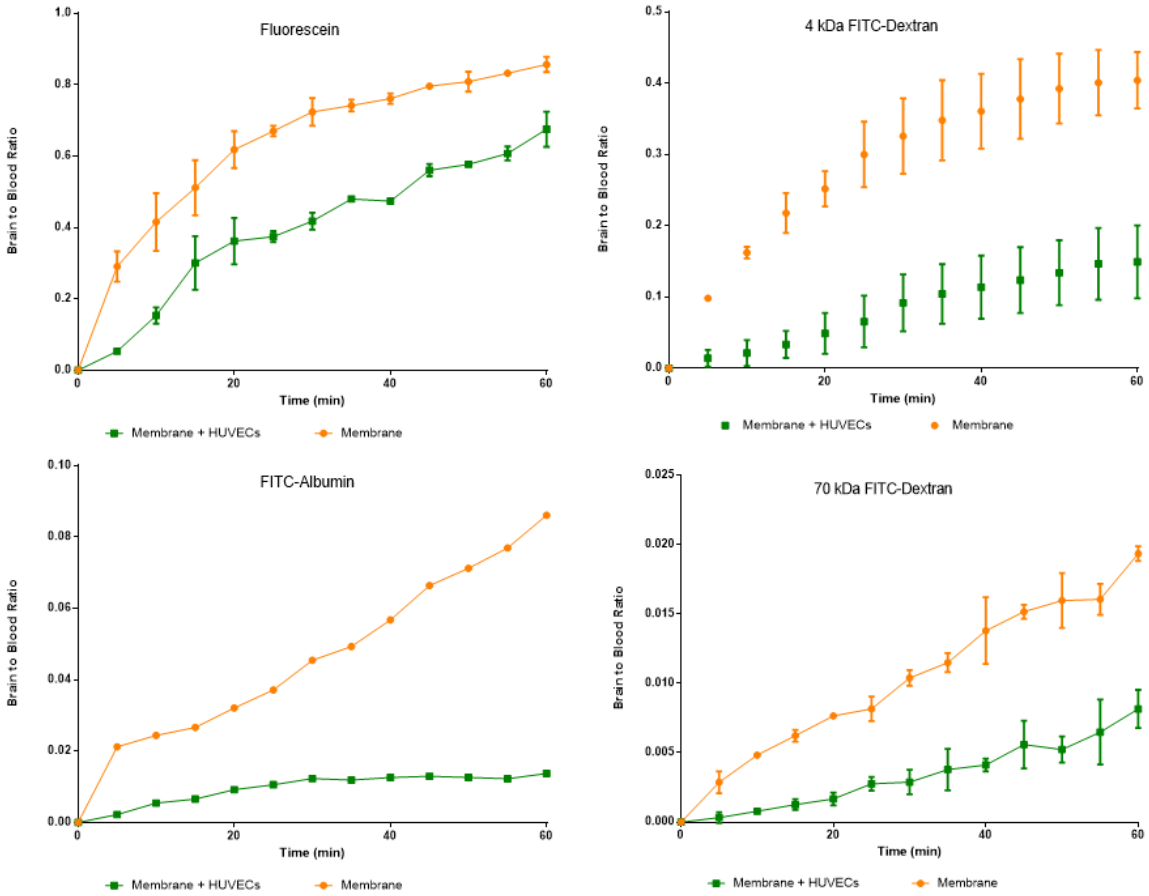

Figure 6. Diffusion of different sized molecules (70 kDa and 4 kDa FITC-dextran, fluorescein and FITC-albumin) across the membrane in the presence and absence of cells. The presence of cells decreased the permeability of the membrane in every case, by 25 % for 4 kDa, 70 kDa dextran, and fluorescein, and approximately 80 % for FITC-albumin.

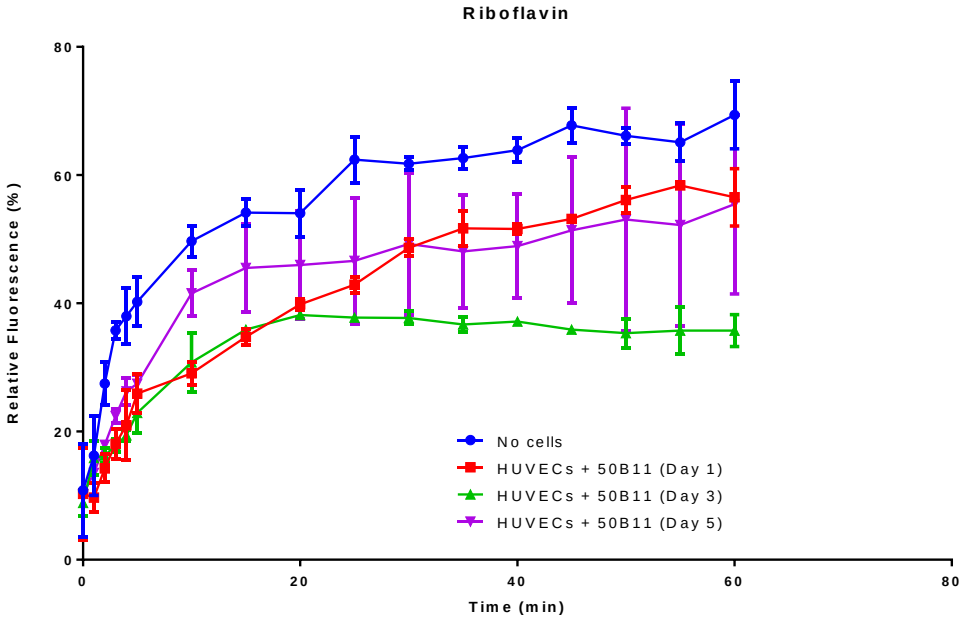

Figure 7. The transport of riboflavin across the BBB in presence of HUVECs and 50B11 cells at different time points.

5.6 IMMUNOSTAINING

Endothelial cells within the BBB are characterized by the formation of intercellular junctions which are of crucial importance for the adhesion and signaling between adjacent cells to maintain the function of the microvessels. These junctions could be organized into three different groups; gap junctions allow the diffusion of small molecular weight substances, adherens junctions, and tight junctions which are critical in order to establish a barrier function. All of these dynamic junctions are formed by different proteins expressed on the endothelial cells. Vascular endothelial cadherin (VE-Cadherin) is a specific protein within the cadherin transmembrane adhesion protein family expressed by only endothelial cells and it is present in all types of vessels [58].

RFP-HUVECs were seeded onto the membrane and were cultured under static conditions for 24 h. Afterwards the cells were fixed and permeabilized prior to the addition of anti-VE-Cadherin primary antibody followed by the incubation with Alexa-488 labelled secondary antibody. Finally, the samples were stained additionally with 4',6-diamidino-2-phenylindole (DAPI), a stain which binds to the denine–thymine rich regions in DNA, therefore can used as a nuclear stain. Our results have shown a uniform distribution and extended morphology of RFP-HUVECs on the membrane after 24 h depicted in the RFP channel. VE-Cadherin accumulated in the intercellular region, suggesting the formation of adherens junctions even after 1 day of culture (**Figure 8**). Although there are still gaps between the cells and the

monolayer is not fully formed, it could possibly be improved by culturing the cells for a longer period of time.

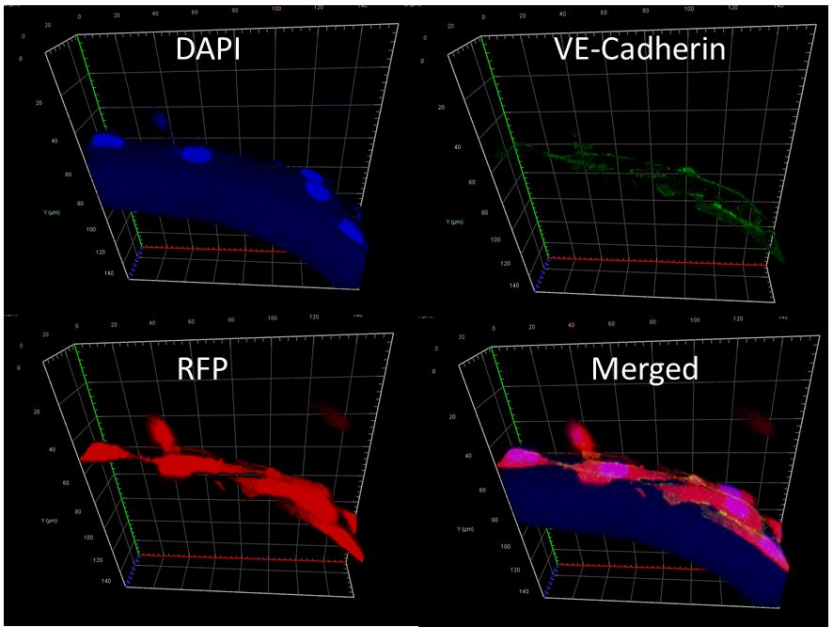

Figure 8. Immunostaining of HUVECs cells on the membrane 24 h after seeding.

6 CONCLUSION

In this project we have demonstrated the fabrication of a novel a BBB model on a chip. A medical grade biocompatible pressure sensitive double-sided tape was used instead of PDMS to produce the mould which can be mounted on high precision glass slide to enable the direct HD bioprinting of the membrane and the optical imaging of the channels. The fast and high-throughput production of hydrogels while maintaining the high resolution of the structures were achieved via 2PP. The BBB was printed directly on the chip without the need of additional assembly step and the residual material could be removed via a single washing step. The membranes can be seeded with different cells without the need of additional coating steps. Both the endothelial cells and dorsal root ganglion cells showed good viability and monolayer formation after 2 day of seeding. The membrane was characterized by the diffusion of different sized molecules across the membrane using different thickness membranes showing no significant differences after 1 h, however, there was a significant difference at later time points when larger molecules were applied. The membrane showed a size dependent perfusion rate of the different

fluorescent substances. When the membrane was seeded with endothelial cells the diffusion rates decreased in all cases, there was a 25 % decrease in the case of fluorescein, 4 kDa FITC-dextran and 70 kDa FITC-dextran and 80 % decrease in the case of FITC-albumin. Immunostaining of the cells suggested the formation of adherens junction formation even after 24 h of cells seeding. We hypothesize that our model can be further enhanced by using brain microvascular endothelial cells together with primary astrocytes and pericytes to improve the barrier function of the device. Literature suggests that glial cells and the interactions between them and endothelial cells are necessary for the induction of BBB function [12]. Additionally, literature suggest that endothelial cell survival and the intercellular junction formation is enhanced upon perfusion [18]. The effect of different shear stresses introduced to the blood compartment of the chip should be evaluated to further optimize the system. Additionally, different immunostainings could be employed to further characterize the intercellular junction formation of the endothelial cells. PECAM is a transmembrane immunoglobulin that can be found in intercellular junctions and it plays an important role in angiogenesis, and the inactivation of the PECAM gene led to an increase of vascular permeability in a mouse model. Tight junctions contain both transmembrane and intracellular proteins and they are responsible for the tight barrier function of the BBB, therefore evaluation of the tight junction formation is of crucial importance in the BBB models [59].

We envision using this technology to create a physiologically relevant glioblastoma-on-a-chip model together with a BBB. The glioblastoma cell spheroids can be formed by aggregating the cells using a no adhesion agarose mould and can be encapsulated into a 3D hydrogel in the brain compartment on the chip (**Figure 9**). The migration and the proliferation of the tumor spheroids can be followed over time. Furthermore, this construct could enable the screening of possible drugs and therapeutics and their transport through the BBB in order to improve the currently available treatment option and delivery strategies and gain more understanding in the disease progression.

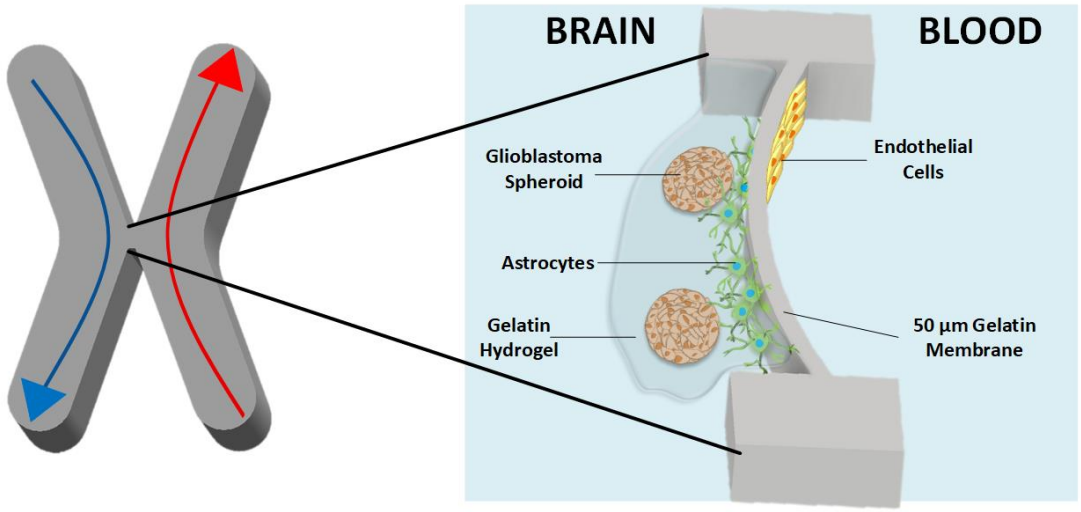

Figure 9. Schematic of a glioblastoma-on-a-chip construct employing the BBB model.

7 ACKNOWLEDGEMENT

Financial support from the Marshall Plan Foundation is gratefully acknowledged. I would like to further thank Jasper Van Hoorick and Prof. Sandra Van Vlierberghe (Ghent University) for providing the Gel-NB that were used throughout this project. I would like to thank Prof. Ali Khademhosseini and Prof. Aleksandr Ovsianikov for the opportunity to carry out this research and his support throughout the project.

8 REFERENCES:

[1] E. Törnqvist, A. Annas, B. Granath, E. Jalkesten, I. Cotgreave, and M. Öberg, "Strategic Focus on 3R Principles Reveals Major Reductions in the Use of Animals in Pharmaceutical Toxicity Testing," *PLoS One*, vol. 9, no. 7, p. e101638, Jul. 2014.

[2] D. Antoni, H. Burckel, E. Josset, and G. Noel, "Three-dimensional cell culture: a breakthrough in vivo.," *Int. J. Mol. Sci.*, vol. 16, no. 3, pp. 5517–27, Mar. 2015.

[3] S. Melissaridou *et al.*, "The effect of 2D and 3D cell cultures on treatment response, EMT profile and stem cell features in head and neck cancer," *Cancer Cell Int.*, vol. 19, no. 1, p. 16, Dec. 2019.

[4] J. Friedrich, C. Seidel, R. Ebner, and L. A. Kunz-Schughart, "Spheroid-based drug screen: considerations and practical approach," *Nat. Protoc.*, vol. 4, no. 3, pp. 309–324, Feb. 2009.

[5] D. Huh, G. A. Hamilton, and D. E. Ingber, "From 3D cell culture to organs-on-chips," *Trends Cell Biol.*, vol. 21, no. 12, pp. 745–754, 2011.

[6] J. P. Wikswo *et al.*, "Engineering challenges for instrumenting and controlling integrated organ-on-chip systems," *IEEE Transactions on Biomedical Engineering*, vol. 60, no. 3. pp. 682–690, 2013.

[7] N. A. O. Bush, S. M. Chang, and M. S. Berger, "Current and future strategies for treatment of glioma," *Neurosurgical Review*, vol. 40, no. 1. Springer Verlag, 01-Jan-2017.

[8] P. Y. Wen and S. Kesari, "Malignant gliomas in adults.," *N. Engl. J. Med.*, vol. 359, no. 5, pp. 492–507, Jul. 2008.

[9] E. Alphandéry, "Glioblastoma treatments: An account of recent industrial developments," *Frontiers in Pharmacology*, vol. 9, no. SEP. Frontiers Media S.A., 13-Sep-2018.

[10] C. Alifieris and D. T. Trafalis, "Glioblastoma multiforme: Pathogenesis and treatment," *Pharmacology and Therapeutics*, vol. 152. Elsevier Inc., pp. 63–82, 29-Jun-2015.

[11] N. J. Abbott, L. Rönnbäck, and E. Hansson, "Astrocyte–endothelial interactions at the blood–brain barrier," *Nat. Rev. Neurosci.*, vol. 7, no. 1, pp. 41–53, Jan. 2006.

[12] R. C. Janzer and M. C. Raff, "Astrocytes induce blood-brain barrier properties in endothelial cells.," *Nature*, vol. 325, no. 6101, pp. 253–7.

[13] K. M. Baeten and K. Akassoglou, "Extracellular matrix and matrix receptors in blood-brain barrier formation and stroke," *Dev. Neurobiol.*, vol. 71, no. 11, pp. 1018–1039, Nov. 2011.

[14] A. Lalatsa and A. M. Butt, "Physiology of the Blood–Brain Barrier and Mechanisms of Transport Across the BBB," *Nanotechnology-Based Target. Drug Deliv. Syst. Brain Tumors*, pp. 49–74, Jan. 2018.

[15] N. J. Abbott, A. A. K. Patabendige, D. E. M. Dolman, S. R. Yusof, and D. J. Begley, "Structure and function of the blood–brain barrier," *Neurobiol. Dis.*, vol. 37, no. 1, pp. 13–25, Jan. 2010.

[16] G. A. Rosenberg, "Neurological diseases in relation to the blood-brain barrier.," *J. Cereb. Blood Flow Metab.*, vol. 32, no. 7, pp. 1139–51, Jul. 2012.

[17] R. Booth and H. Kim, "Characterization of a microfluidic in vitro model of the blood-brain barrier (μBBB)," *Lab Chip*, vol. 12, no. 10, pp. 1784–1792, Apr. 2012.

[18] L. M. Griep *et al.*, "BBB on CHIP: Microfluidic platform to mechanically and biochemically modulate

blood-brain barrier function," *Biomed. Microdevices*, vol. 15, no. 1, pp. 145–150, Feb. 2013.

[19] J. A. Kim, H. N. Kim, S.-K. Im, S. Chung, J. Y. Kang, and N. Choi, "Collagen-based brain microvasculature model in vitro using three-dimensional printed template.," *Biomicrofluidics*, vol. 9, no. 2, p. 024115, Mar. 2015.

[20] A. K. H. Achyuta *et al.*, "A modular approach to create a neurovascular unit-on-a-chip," *Lab Chip*, vol. 13, no. 4, pp. 542–553, Feb. 2013.

[21] S. H. Ma, L. A. Lepak, R. J. Hussain, W. Shain, and M. L. Shuler, "An endothelial and astrocyte co-culture model of the blood–brain barrier utilizing an ultra-thin, nanofabricated silicon nitride membrane," *Lab Chip*, vol. 5, no. 1, pp. 74–85, Dec. 2005.

[22] J. A. Brown *et al.*, "Recreating blood-brain barrier physiology and structure on chip: A novel neurovascular microfluidic bioreactor," *Biomicrofluidics*, vol. 9, no. 5, p. 054124, Sep. 2015.

[23] S. P. Deosarkar, B. Prabhakarpandian, B. Wang, J. B. Sheffield, B. Krynska, and M. F. Kiani, "A Novel Dynamic Neonatal Blood-Brain Barrier on a Chip," *PLoS One*, vol. 10, no. 11, p. e0142725, Nov. 2015.

[24] Y. I. Wang, H. E. Abaci, and M. L. Shuler, "Microfluidic blood-brain barrier model provides in vivo-like barrier properties for drug permeability screening," *Biotechnol. Bioeng.*, vol. 114, no. 1, pp. 184–194, Jan. 2017.

[25] M. Akay *et al.*, "Drug Screening of Human GBM Spheroids in Brain Cancer Chip," *Sci. Rep.*, vol. 8, no. 1, Dec. 2018.

[26] Y. Fan, D. T. Nguyen, Y. Akay, F. Xu, and M. Akay, "Engineering a Brain Cancer Chip for High-throughput Drug Screening," *Sci. Rep.*, vol. 6, May 2016.

[27] J. M. Ayuso *et al.*, "Glioblastoma on a microfluidic chip: Generating pseudopalisades and enhancing aggressiveness through blood vessel obstruction events," *Neuro. Oncol.*, vol. 19, no. 4, pp. 503–513, Apr. 2017.

[28] H.-G. Yi *et al.*, "A bioprinted human-glioblastoma-on-a-chip for the identification of patient-specific responses to chemoradiotherapy," *Nat. Biomed. Eng.*, p. 1, Mar. 2019.

[29] J. E. Sosa-Hernández *et al.*, "Organs-on-a-chip module: A review from the development and applications perspective," *Micromachines*, vol. 9, no. 10. MDPI AG, 22-Oct-2018.

[30] D. A. Mair, E. Geiger, A. P. Pisano, J. M. J. Fréchet, and F. Svec, "Injection molded microfluidic chips featuring integrated interconnects," *Lab Chip*, vol. 6, no. 10, pp. 1346–1354, 2006.

[31] E. A. Waddell, "Laser Ablation as a Fabrication Technique for Microfluidic Devices BT - Microfluidic Techniques: Reviews and Protocols," S. D. Minteer, Ed. Humana Press, 2006, pp. 27–38.

[32] H. Becker and U. Heim, "Hot embossing as a method for the fabrication of polymer high aspect ratio structures," *Sensors Actuators, A Phys.*, vol. 83, no. 1, pp. 130–135, May 2000.

[33] S. Tasoglu and U. Demirci, "Bioprinting for stem cell research.," *Trends Biotechnol.*, vol. 31, no. 1, pp. 10–9, Jan. 2013.

[34] S. V Murphy and A. Atala, "3D bioprinting of tissues and organs," *Nat. Biotechnol.*, vol. 32, no. 8, pp. 773–785, Aug. 2014.

[35] A. Ovsianikov *et al.*, "Laser fabrication of three-dimensional CAD scaffolds from photosensitive gelatin for applications in tissue engineering," *Biomacromolecules*, vol. 12, no. 4, pp. 851–858, 2011.

[36] M. Kobayashi and H. S. Hyu, "Development and evaluation of polyvinyl alcohol-hydrogels as an artificial atrticular cartilage for orthopedic implants," *Materials (Basel).*, vol. 3, no. 4, pp. 2753–2771, 2010.

[37] R. Bellucci, "An introduction to intraocular lenses: Material, optics, haptics, design and aberration," *Cataract*, vol. 3, pp. 38–55, 2013.

[38] M. F. Maitz, "Applications of synthetic polymers in clinical medicine," *Biosurface and Biotribology*, vol. 1, no. 3, pp. 161–176, 2015.

[39] J. Zhu and R. E. Marchant, "Design properties of hydrogel tissue-engineering scaffolds.," *Expert Rev. Med. Devices*, vol. 8, no. 5, pp. 607–26, 2011.

[40] M. Tromayer *et al.*, "A biocompatible macromolecular two-photon initiator based on hyaluronan.," *Polym. Chem.*, vol. 8, no. 2, pp. 451–460, Jan. 2017.

[41] M. Tromayer *et al.*, "A biocompatible diazosulfonate initiator for direct encapsulation of human stem cells *via* two-photon polymerization," *Polym. Chem.*, vol. 9, no. 22, pp. 3108–3117, Jun. 2018.

[42] C. E. Hoyle and C. N. Bowman, "Thiol-Ene Click Chemistry," *Angew. Chemie Int. Ed.*, vol. 49, no. 9, pp. 1540–1573, Feb. 2010.

[43] J. Van Hoorick *et al.*, "Highly Reactive Thiol-Norbornene Photo-Click Hydrogels : Toward Improved Processability," *Macromol. Rapid Commun.*, vol. 39, no. 14, p. 1800181, 2018.

[44] W. R. Zipfel, R. M. Williams, and W. W. Webb, "Nonlinear magic: multiphoton microscopy in the biosciences," *Nat. Biotechnol.*, vol. 21, no. 11, pp. 1369–1377, 2003.

[45] S. L. Peterson, A. McDonald, P. L. Gourley, and D. Y. Sasaki, "Poly(dimethylsiloxane) thin films as biocompatible coatings for microfluidic devices: Cell culture and flow studies with glial cells," *J. Biomed. Mater. Res.*, vol. 72A, no. 1, pp. 10–18, Jan. 2005.

[46] A. Piruska *et al.*, "The autofluorescence of plastic materials and chips measured under laser irradiation," *Lab Chip*, vol. 5, no. 12, p. 1348, Dec. 2005.

[47] M. W. Toepke and D. J. Beebe, "PDMS absorption of small molecules and consequences in microfluidic applications," *Lab Chip*, vol. 6, no. 12, p. 1484, Dec. 2006.

[48] A. L. Paguirigan and D. J. Beebe, "From the cellular perspective: exploring differences in the cellular baseline in macroscale and microfluidic cultures.," *Integr. Biol. (Camb).*, vol. 1, no. 2, pp. 182–95, Feb. 2009.

[49] A. Dobos *et al.*, "Thiol–Gelatin–Norbornene Bioink for Laser-Based High-Definition Bioprinting," *Adv. Healthc. Mater.*, 2019.

[50] H. Wen, J. Hao, and S. K. Li, "Characterization of Human Sclera Barrier Properties for Transscleral Delivery of Bevacizumab and Ranibizumab," *J. Pharm. Sci.*, vol. 102, no. 3, p. 892, Mar. 2013.

[51] Z. Chen, B. Krishnamachary, M.-F. Penet, and Z. M. Bhujwalla, "Acid-degradable Dextran as an Image Guided siRNA Carrier for COX-2 Downregulation," *Theranostics*, vol. 8, no. 1, pp. 1–12, 2018.

[52] A. K. Bloom, M. L. Samsom, S. C. Regmi, B. L. Steele, and T. A. Schmidt, "Investigating the effect of proteoglycan 4 on hyaluronan solution properties using confocal fluorescence recovery after photobleaching," *BMC Musculoskelet. Disord.*, vol. 20, no. 1, p. 93, Dec. 2019.

[53] S. Sadasivan, M. Zanin, K. O'Brien, S. Schultz-Cherry, and R. J. Smeyne, "Induction of Microglia Activation after Infection with the Non-Neurotropic A/CA/04/2009 H1N1 Influenza Virus," *PLoS One*, vol. 10, no. 4, p. e0124047, Apr. 2015.

[54] S. Gustafsson *et al.*, "Blood-brain barrier integrity in a mouse model of Alzheimer's disease with or without acute 3D6 immunotherapy," *Neuropharmacology*, vol. 143, pp. 1–9, Dec. 2018.

[55] A. Manaenko, H. Chen, J. Kammer, J. H. Zhang, and J. Tang, "Comparison Evans Blue injection routes: Intravenous versus intraperitoneal, for measurement of blood–brain barrier in a mice hemorrhage model," *J. Neurosci. Methods*, vol. 195, no. 2, pp. 206–210, Feb. 2011.

[56] C.-J. Xu *et al.*, "Evaluation of blood-brain barrier permeability in tryptophan hydroxylase 2-knockout mice.," *Exp. Ther. Med.*, vol. 8, no. 5, pp. 1467–1470, Nov. 2014.

[57] M. Patel, R. K. Vadlapatla, D. Pal, and A. K. Mitra, "Molecular and functional characterization of riboflavin specific transport system in rat brain capillary endothelial cells.," *Brain Res.*, vol. 1468, pp. 1–10, Aug. 2012.

[58] G. Bazzoni and E. Dejana, "Endothelial Cell-to-Cell Junctions: Molecular Organization and Role in Vascular Homeostasis," *Physiol. Rev.*, vol. 84, no. 3, pp. 869–901, Jul. 2004.

[59] J. M. Anderson and C. M. Van Itallie, "Physiology and function of the tight junction.," *Cold Spring Harb. Perspect. Biol.*, vol. 1, no. 2, p. a002584, Aug. 2009.